FERMILAB-PUB-10-325-E

Search for $ZH \to \ell^+\ell^- b\bar{b}$ production in 4.2 fb^{-1} of $p\bar{p}$ collisions at $\sqrt{s} = 1.96$ TeV

V.M. Abazov,[35] B. Abbott,[73] M. Abolins,[62] B.S. Acharya,[29] M. Adams,[48] T. Adams,[46] G.D. Alexeev,[35] G. Alkhazov,[39] A. Alton[a],[61] G. Alverson,[60] G.A. Alves,[2] L.S. Ancu,[34] M. Aoki,[47] Y. Arnoud,[14] M. Arov,[57] A. Askew,[46] B. Åsman,[40] O. Atramentov,[65] C. Avila,[8] J. BackusMayes,[80] F. Badaud,[13] L. Bagby,[47] B. Baldin,[47] D.V. Bandurin,[46] S. Banerjee,[29] E. Barberis,[60] P. Baringer,[55] J. Barreto,[2] J.F. Bartlett,[47] U. Bassler,[18] S. Beale,[6] A. Bean,[55] M. Begalli,[3] M. Begel,[71] C. Belanger-Champagne,[40] L. Bellantoni,[47] J.A. Benitez,[62] S.B. Beri,[27] G. Bernardi,[17] R. Bernhard,[22] I. Bertram,[41] M. Besançon,[18] R. Beuselinck,[42] V.A. Bezzubov,[38] P.C. Bhat,[47] V. Bhatnagar,[27] G. Blazey,[49] S. Blessing,[46] K. Bloom,[64] A. Boehnlein,[47] D. Boline,[70] T.A. Bolton,[56] E.E. Boos,[37] G. Borissov,[41] T. Bose,[59] A. Brandt,[76] O. Brandt,[23] R. Brock,[62] G. Brooijmans,[68] A. Bross,[47] D. Brown,[17] J. Brown,[17] X.B. Bu,[7] D. Buchholz,[50] M. Buehler,[79] V. Buescher,[24] V. Bunichev,[37] S. Burdin[b],[41] T.H. Burnett,[80] C.P. Buszello,[42] B. Calpas,[15] S. Calvet,[16] E. Camacho-Pérez,[32] M.A. Carrasco-Lizarraga,[32] E. Carrera,[46] B.C.K. Casey,[47] H. Castilla-Valdez,[32] S. Chakrabarti,[70] D. Chakraborty,[49] K.M. Chan,[53] A. Chandra,[78] G. Chen,[55] S. Chevalier-Théry,[18] D.K. Cho,[75] S.W. Cho,[31] S. Choi,[31] B. Choudhary,[28] T. Christoudias,[42] S. Cihangir,[47] D. Claes,[64] J. Clutter,[55] M. Cooke,[47] W.E. Cooper,[47] M. Corcoran,[78] F. Couderc,[18] M.-C. Cousinou,[15] A. Croc,[18] D. Cutts,[75] M. Ćwiok,[30] A. Das,[44] G. Davies,[42] K. De,[76] S.J. de Jong,[34] E. De La Cruz-Burelo,[32] F. Déliot,[18] M. Demarteau,[47] R. Demina,[69] D. Denisov,[47] S.P. Denisov,[38] S. Desai,[47] K. DeVaughan,[64] H.T. Diehl,[47] M. Diesburg,[47] A. Dominguez,[64] T. Dorland,[80] A. Dubey,[28] L.V. Dudko,[37] D. Duggan,[65] A. Duperrin,[15] S. Dutt,[27] A. Dyshkant,[49] M. Eads,[64] D. Edmunds,[62] J. Ellison,[45] V.D. Elvira,[47] Y. Enari,[17] S. Eno,[58] H. Evans,[51] A. Evdokimov,[71] V.N. Evdokimov,[38] G. Facini,[60] A.V. Ferapontov,[75] T. Ferbel,[58,69] F. Fiedler,[24] F. Filthaut,[34] W. Fisher,[62] H.E. Fisk,[47] M. Fortner,[49] H. Fox,[41] S. Fuess,[47] T. Gadfort,[71] A. Garcia-Bellido,[69] V. Gavrilov,[36] P. Gay,[13] W. Geist,[19] W. Geng,[15,62] D. Gerbaudo,[66] C.E. Gerber,[48] Y. Gershtein,[65] G. Ginther,[47,69] G. Golovanov,[35] A. Goussiou,[80] P.D. Grannis,[70] S. Greder,[19] H. Greenlee,[47] Z.D. Greenwood,[57] E.M. Gregores,[4] G. Grenier,[20] Ph. Gris,[13] J.-F. Grivaz,[16] A. Grohsjean,[18] S. Grünendahl,[47] M.W. Grünewald,[30] F. Guo,[70] J. Guo,[70] G. Gutierrez,[47] P. Gutierrez,[73] A. Haas[c],[68] S. Hagopian,[46] J. Haley,[60] L. Han,[7] K. Harder,[43] A. Harel,[69] J.M. Hauptman,[54] J. Hays,[42] T. Hebbeker,[21] D. Hedin,[49] H. Hegab,[74] A.P. Heinson,[45] U. Heintz,[75] C. Hensel,[23] I. Heredia-De La Cruz,[32] K. Herner,[61] G. Hesketh,[60] M.D. Hildreth,[53] R. Hirosky,[79] T. Hoang,[46] J.D. Hobbs,[70] B. Hoeneisen,[12] M. Hohlfeld,[24] S. Hossain,[73] Z. Hubacek,[10] N. Huske,[17] V. Hynek,[10] I. Iashvili,[67] R. Illingworth,[47] A.S. Ito,[47] S. Jabeen,[75] M. Jaffré,[16] S. Jain,[67] D. Jamin,[15] R. Jesik,[42] K. Johns,[44] M. Johnson,[47] D. Johnston,[64] A. Jonckheere,[47] P. Jonsson,[42] J. Joshi,[27] A. Juste[d],[47] K. Kaadze,[56] E. Kajfasz,[15] D. Karmanov,[37] P.A. Kasper,[47] I. Katsanos,[64] R. Kehoe,[77] S. Kermiche,[15] N. Khalatyan,[47] A. Khanov,[74] A. Kharchilava,[67] Y.N. Kharzheev,[35] D. Khatidze,[75] M.H. Kirby,[50] J.M. Kohli,[27] A.V. Kozelov,[38] J. Kraus,[62] A. Kumar,[67] A. Kupco,[11] T. Kurča,[20] V.A. Kuzmin,[37] J. Kvita,[9] S. Lammers,[51] G. Landsberg,[75] P. Lebrun,[20] H.S. Lee,[31] S.W. Lee,[54] W.M. Lee,[47] J. Lellouch,[17] L. Li,[45] Q.Z. Li,[47] S.M. Lietti,[5] J.K. Lim,[31] D. Lincoln,[47] J. Linnemann,[62] V.V. Lipaev,[38] R. Lipton,[47] Y. Liu,[7] Z. Liu,[6] A. Lobodenko,[39] M. Lokajicek,[11] P. Love,[41] H.J. Lubatti,[80] R. Luna-Garcia[e],[32] A.L. Lyon,[47] A.K.A. Maciel,[2] D. Mackin,[78] R. Madar,[18] R. Magaña-Villalba,[32] S. Malik,[64] V.L. Malyshev,[35] Y. Maravin,[56] J. Martínez-Ortega,[32] R. McCarthy,[70] C.L. McGivern,[55] M.M. Meijer,[34] A. Melnitchouk,[63] D. Menezes,[49] P.G. Mercadante,[4] M. Merkin,[37] A. Meyer,[21] J. Meyer,[23] N.K. Mondal,[29] G.S. Muanza,[15] M. Mulhearn,[79] E. Nagy,[15] M. Naimuddin,[28] M. Narain,[75] R. Nayyar,[28] H.A. Neal,[61] J.P. Negret,[8] P. Neustroev,[39] H. Nilsen,[22] S.F. Novaes,[5] T. Nunnemann,[25] G. Obrant,[39] D. Onoprienko,[56] J. Orduna,[32] N. Osman,[42] J. Osta,[53] G.J. Otero y Garzón,[1] M. Owen,[43] M. Padilla,[45] M. Pangilinan,[75] N. Parashar,[52] V. Parihar,[75] S.K. Park,[31] J. Parsons,[68] R. Partridge[c],[75] N. Parua,[51] A. Patwa,[71] B. Penning,[47] M. Perfilov,[37] K. Peters,[43] Y. Peters,[43] G. Petrillo,[69] P. Pétroff,[16] R. Piegaia,[1] J. Piper,[62] M.-A. Pleier,[71] P.L.M. Podesta-Lerma[f],[32] V.M. Podstavkov,[47] M.-E. Pol,[2] P. Polozov,[36] A.V. Popov,[38] M. Prewitt,[78] D. Price,[51] S. Protopopescu,[71] J. Qian,[61] A. Quadt,[23] B. Quinn,[63] M.S. Rangel,[16] K. Ranjan,[28] P.N. Ratoff,[41] I. Razumov,[38] P. Renkel,[77] P. Rich,[43] M. Rijssenbeek,[70] I. Ripp-Baudot,[19] F. Rizatdinova,[74] M. Rominsky,[47] C. Royon,[18] P. Rubinov,[47] R. Ruchti,[53] G. Safronov,[36] G. Sajot,[14] A. Sánchez-Hernández,[32] M.P. Sanders,[25] B. Sanghi,[47] A.S. Santos,[5] G. Savage,[47] L. Sawyer,[57] T. Scanlon,[42] R.D. Schamberger,[70] Y. Scheglov,[39] H. Schellman,[50] T. Schliephake,[26] S. Schlobohm,[80] C. Schwanenberger,[43] R. Schwienhorst,[62] J. Sekaric,[55] H. Severini,[73] E. Shabalina,[23] V. Shary,[18] A.A. Shchukin,[38] R.K. Shivpuri,[28] V. Simak,[10] V. Sirotenko,[47] P. Skubic,[73] P. Slattery,[69] D. Smirnov,[53] K.J. Smith,[67] G.R. Snow,[64] J. Snow,[72] S. Snyder,[71] S. Söldner-Rembold,[43] L. Sonnenschein,[21] A. Sopczak,[41]

M. Sosebee,[76] K. Soustruznik,[9] B. Spurlock,[76] J. Stark,[14] V. Stolin,[36] D.A. Stoyanova,[38] E. Strauss,[70] M. Strauss,[73] D. Strom,[48] L. Stutte,[47] P. Svoisky,[34] M. Takahashi,[43] A. Tanasijczuk,[1] W. Taylor,[6] M. Titov,[18] V.V. Tokmenin,[35] D. Tsybychev,[70] B. Tuchming,[18] C. Tully,[66] P.M. Tuts,[68] L. Uvarov,[39] S. Uvarov,[39] S. Uzunyan,[49] R. Van Kooten,[51] W.M. van Leeuwen,[33] N. Varelas,[48] E.W. Varnes,[44] I.A. Vasilyev,[38] P. Verdier,[20] L.S. Vertogradov,[35] M. Verzocchi,[47] M. Vesterinen,[43] D. Vilanova,[18] P. Vint,[42] P. Vokac,[10] H.D. Wahl,[46] M.H.L.S. Wang,[69] J. Warchol,[53] G. Watts,[80] M. Wayne,[53] M. Weber[g],[47] M. Wetstein,[58] A. White,[76] D. Wicke,[24] M.R.J. Williams,[41] G.W. Wilson,[55] S.J. Wimpenny,[45] M. Wobisch,[57] D.R. Wood,[60] T.R. Wyatt,[43] Y. Xie,[47] C. Xu,[61] S. Yacoob,[50] R. Yamada,[47] W.-C. Yang,[43] T. Yasuda,[47] Y.A. Yatsunenko,[35] Z. Ye,[47] H. Yin,[7] K. Yip,[71] H.D. Yoo,[75] S.W. Youn,[47] J. Yu,[76] S. Zelitch,[79] T. Zhao,[80] B. Zhou,[61] J. Zhu,[61] M. Zielinski,[69] D. Zieminska,[51] and L. Zivkovic[68]

(The D0 Collaboration)

[1]*Universidad de Buenos Aires, Buenos Aires, Argentina*
[2]*LAFEX, Centro Brasileiro de Pesquisas Físicas, Rio de Janeiro, Brazil*
[3]*Universidade do Estado do Rio de Janeiro, Rio de Janeiro, Brazil*
[4]*Universidade Federal do ABC, Santo André, Brazil*
[5]*Instituto de Física Teórica, Universidade Estadual Paulista, São Paulo, Brazil*
[6]*Simon Fraser University, Vancouver, British Columbia, and York University, Toronto, Ontario, Canada*
[7]*University of Science and Technology of China, Hefei, People's Republic of China*
[8]*Universidad de los Andes, Bogotá, Colombia*
[9]*Charles University, Faculty of Mathematics and Physics, Center for Particle Physics, Prague, Czech Republic*
[10]*Czech Technical University in Prague, Prague, Czech Republic*
[11]*Center for Particle Physics, Institute of Physics, Academy of Sciences of the Czech Republic, Prague, Czech Republic*
[12]*Universidad San Francisco de Quito, Quito, Ecuador*
[13]*LPC, Université Blaise Pascal, CNRS/IN2P3, Clermont, France*
[14]*LPSC, Université Joseph Fourier Grenoble 1, CNRS/IN2P3, Institut National Polytechnique de Grenoble, Grenoble, France*
[15]*CPPM, Aix-Marseille Université, CNRS/IN2P3, Marseille, France*
[16]*LAL, Université Paris-Sud, CNRS/IN2P3, Orsay, France*
[17]*LPNHE, Universités Paris VI and VII, CNRS/IN2P3, Paris, France*
[18]*CEA, Irfu, SPP, Saclay, France*
[19]*IPHC, Université de Strasbourg, CNRS/IN2P3, Strasbourg, France*
[20]*IPNL, Université Lyon 1, CNRS/IN2P3, Villeurbanne, France and Université de Lyon, Lyon, France*
[21]*III. Physikalisches Institut A, RWTH Aachen University, Aachen, Germany*
[22]*Physikalisches Institut, Universität Freiburg, Freiburg, Germany*
[23]*II. Physikalisches Institut, Georg-August-Universität Göttingen, Göttingen, Germany*
[24]*Institut für Physik, Universität Mainz, Mainz, Germany*
[25]*Ludwig-Maximilians-Universität München, München, Germany*
[26]*Fachbereich Physik, Bergische Universität Wuppertal, Wuppertal, Germany*
[27]*Panjab University, Chandigarh, India*
[28]*Delhi University, Delhi, India*
[29]*Tata Institute of Fundamental Research, Mumbai, India*
[30]*University College Dublin, Dublin, Ireland*
[31]*Korea Detector Laboratory, Korea University, Seoul, Korea*
[32]*CINVESTAV, Mexico City, Mexico*
[33]*FOM-Institute NIKHEF and University of Amsterdam/NIKHEF, Amsterdam, The Netherlands*
[34]*Radboud University Nijmegen/NIKHEF, Nijmegen, The Netherlands*
[35]*Joint Institute for Nuclear Research, Dubna, Russia*
[36]*Institute for Theoretical and Experimental Physics, Moscow, Russia*
[37]*Moscow State University, Moscow, Russia*
[38]*Institute for High Energy Physics, Protvino, Russia*
[39]*Petersburg Nuclear Physics Institute, St. Petersburg, Russia*
[40]*Stockholm University, Stockholm and Uppsala University, Uppsala, Sweden*
[41]*Lancaster University, Lancaster LA1 4YB, United Kingdom*
[42]*Imperial College London, London SW7 2AZ, United Kingdom*
[43]*The University of Manchester, Manchester M13 9PL, United Kingdom*
[44]*University of Arizona, Tucson, Arizona 85721, USA*
[45]*University of California Riverside, Riverside, California 92521, USA*
[46]*Florida State University, Tallahassee, Florida 32306, USA*
[47]*Fermi National Accelerator Laboratory, Batavia, Illinois 60510, USA*
[48]*University of Illinois at Chicago, Chicago, Illinois 60607, USA*

[49]Northern Illinois University, DeKalb, Illinois 60115, USA
[50]Northwestern University, Evanston, Illinois 60208, USA
[51]Indiana University, Bloomington, Indiana 47405, USA
[52]Purdue University Calumet, Hammond, Indiana 46323, USA
[53]University of Notre Dame, Notre Dame, Indiana 46556, USA
[54]Iowa State University, Ames, Iowa 50011, USA
[55]University of Kansas, Lawrence, Kansas 66045, USA
[56]Kansas State University, Manhattan, Kansas 66506, USA
[57]Louisiana Tech University, Ruston, Louisiana 71272, USA
[58]University of Maryland, College Park, Maryland 20742, USA
[59]Boston University, Boston, Massachusetts 02215, USA
[60]Northeastern University, Boston, Massachusetts 02115, USA
[61]University of Michigan, Ann Arbor, Michigan 48109, USA
[62]Michigan State University, East Lansing, Michigan 48824, USA
[63]University of Mississippi, University, Mississippi 38677, USA
[64]University of Nebraska, Lincoln, Nebraska 68588, USA
[65]Rutgers University, Piscataway, New Jersey 08855, USA
[66]Princeton University, Princeton, New Jersey 08544, USA
[67]State University of New York, Buffalo, New York 14260, USA
[68]Columbia University, New York, New York 10027, USA
[69]University of Rochester, Rochester, New York 14627, USA
[70]State University of New York, Stony Brook, New York 11794, USA
[71]Brookhaven National Laboratory, Upton, New York 11973, USA
[72]Langston University, Langston, Oklahoma 73050, USA
[73]University of Oklahoma, Norman, Oklahoma 73019, USA
[74]Oklahoma State University, Stillwater, Oklahoma 74078, USA
[75]Brown University, Providence, Rhode Island 02912, USA
[76]University of Texas, Arlington, Texas 76019, USA
[77]Southern Methodist University, Dallas, Texas 75275, USA
[78]Rice University, Houston, Texas 77005, USA
[79]University of Virginia, Charlottesville, Virginia 22901, USA
[80]University of Washington, Seattle, Washington 98195, USA

(Dated: August 20, 2010)

We present a search for the standard model Higgs boson produced in association with a Z boson in 4.2 fb^{-1} of $p\bar{p}$ collisions, collected with the D0 detector at the Fermilab Tevatron at $\sqrt{s} = 1.96$ TeV. Selected events contain one reconstructed $Z \to \ell^+\ell^-$ candidate and at least two jets, including at least one b-tagged jet. In the absence of an excess over the background expected from other standard model processes, limits on the ZH cross section multiplied by the branching ratios are set. The limit at $M_H = 115$ GeV is a factor of 5.9 larger than the standard model prediction.

PACS numbers: 14.80.Bn, 13.85.Qk, 13.85.Rm

In the standard model (SM), the spontaneous breakdown of the electroweak gauge symmetry generates masses for the W and Z bosons and produces a scalar massive particle, the Higgs boson, which has so far eluded detection. The discovery of the Higgs boson would top a remarkable list of experimentally confirmed SM predictions.

For Higgs boson masses M_H below 135 GeV, the primary Higgs boson decay in the SM is $H \to b\bar{b}$, which is challenging to discern amidst copious $b\bar{b}$ production at the Tevatron $p\bar{p}$ collider. Consequently, sensitivity to a low-mass Higgs boson is predominantly from its production in association with a W or Z boson that decays to leptons.

In this Letter, we present a search for $ZH \to \ell^+\ell^- b\bar{b}$, where ℓ is either a muon or an electron. The searches for $ZH \to \nu\bar{\nu}b\bar{b}$ and $ZH \to \tau^+\tau^- b\bar{b}$ are treated elsewhere [1, 2]. For the $\ell^+\ell^- b\bar{b}$ final states, the D0 collaboration has previously used 0.45 fb^{-1} of integrated luminosity to report a cross section upper limit at the 95% CL that was around 25 times larger than the SM prediction at $M_H = 115$ GeV [3], and the CDF collaboration

used 2.7 fb^{-1} to obtain a factor of around 8 [4].

The data for this analysis were collected at the Fermilab Tevatron Collider with the D0 detector [5]. After imposing data quality requirements, the integrated luminosity is 4.2 fb^{-1}. The selected events were predominantly acquired by triggers that provide real-time identification of electron and muon candidates, but to maximize acceptance, events from all available triggers are considered.

The selection of signal-like events requires a primary $p\bar{p}$ interaction vertex (PV) that has at least three associated tracks and is located within 60 cm of the center of the detector along the direction of the beam. Selected events must also contain a Z boson candidate with a dilepton invariant mass $60 < m_{\ell\ell} < 150$ GeV.

The dimuon ($\mu\mu$) selection requires at least two muons matched to central tracks with transverse momenta $p_{\rm T} > 10$ GeV. Combined tracking and calorimeter isolation requirements are applied to the muon pair such that one muon does not need to be isolated if the other is sufficiently well isolated. For each muon track, the pseudorapidity $\eta_{\rm det}$, measured with respect to the center of the detector, must satisfy $|\eta_{\rm det}| < 2$ [6]. At least one muon must have $|\eta_{\rm det}| < 1.5$ and $p_{\rm T} > 15$ GeV. The distance of closest approach of each track to the PV in the plane transverse to the beam direction, $d_{\rm PV}$, must be less than 0.02 cm for tracks with at least one hit in the silicon microstrip tracker (SMT). A track without SMT hits must have $d_{\rm PV} < 0.2$ cm, and its $p_{\rm T}$ is corrected through a constraint to the position of the PV. An additional dimuon selection, $\mu\mu_{\rm trk}$, requires one identified muon and one isolated track ($\mu_{\rm trk}$) in the central tracking detector with $p_{\rm T} > 20$ GeV and $|\eta_{\rm det}| < 2$, at least one hit in the SMT, and $d_{\rm PV} < 0.02$ cm [7]. The $\mu_{\rm trk}$ must be separated in pseudorapidity η and azimuth ϕ by $\Delta\mathcal{R} = \sqrt{(\Delta\eta)^2 + (\Delta\phi)^2} > 0.1$ from the other muon. The $\mu\mu_{\rm trk}$ selection adds 10% signal acceptance to the $\mu\mu$ selection, mainly from gaps in the muon detector. To reduce contamination from cosmic rays, the tracks from both selections must not be back-to-back in η and ϕ. The two muons must also have opposite charge.

The dielectron (ee) selection requires at least two electrons of $p_{\rm T} > 15$ GeV identified by electromagnetic showers in the calorimeter. Each shower must be isolated from other energy depositions and have a shape consistent with that expected of an electron. At least one electron must be identified in the central calorimeter (CC, $|\eta_{\rm det}| < 1.1$), and a second electron either in the CC or the end calorimeter (EC, $1.5 < |\eta_{\rm det}| < 2.5$). The CC electrons must match central tracks or produce a pattern of hits in the tracker consistent with that expected of an electron. An additional dielectron selection, $ee_{\rm ICR}$, requires exactly one electron from the CC or EC, with a second electron identified as a narrow calorimeter cluster in the inter-cryostat region (ICR, $1.1 < |\eta_{\rm det}| < 1.5$) with a matching track in the central tracker [8]. A neural network ($\rm NN_{ICR}$) is used to differentiate ICR electrons from jets. The $ee_{\rm ICR}$ selection requires an explicit single-electron trigger, and adds 17% signal acceptance to the ee selection.

Jets are reconstructed in the calorimeter using the iterative midpoint cone algorithm [9] with a cone of radius 0.5. The energy scale of jets is corrected for detector response, the presence of noise and multiple $p\bar{p}$ interactions, and energy deposited outside of the reconstructed jet cone. At least two jets with $|\eta_{\rm det}| < 2.5$ are required, with the leading jet of $p_{\rm T} > 20$ GeV and additional jets of $p_{\rm T} > 15$ GeV. Both electrons in dielectron events are required to be isolated from any jet by $\Delta\mathcal{R} > 0.5$. Likewise, jets must be separated by $\Delta\mathcal{R} > 0.5$ from the $\mu_{\rm trk}$ candidate in the $\mu\mu_{\rm trk}$ channel, but no such requirement is applied to the muon candidates in either dimuon channel. To reduce the impact from multiple $p\bar{p}$ interactions at high instantaneous luminosities, jets must contain at least two tracks matched to the PV.

To distinguish the decay $H \to b\bar{b}$ from background processes involving light quarks and gluons, jets are identified as likely containing b-quarks (b-tagged) if they pass loose or tight requirements on the output of a neural network trained to separate b-jets from light jets [10]. For $|\eta| < 0.7$ and $p_{\rm T} > 45$ GeV, the b-tagging efficiency for b-jets and the misidentification rate of light jets are, respectively, 74% and 8.5% for loose b-tags, and 48% and 0.6% for tight b-tags. Events with at least two loose b-tags are classified as double-tagged (DT). Events not in the DT sample that contain a single tight b-tag are classified as single-tagged (ST). The dijet $H \to b\bar{b}$ candidate is composed of the two highest $p_{\rm T}$ b-tagged jets in DT events, and the b-tagged jet plus the highest $p_{\rm T}$ non-b-tagged jet in ST events.

The background from multijet events with jets misidentified as leptons is estimated from control samples in the data. For the $\mu\mu$ channel, the multijet control sample contains events that fail the muon isolation requirement but otherwise pass the event selection. In the $\mu\mu_{\rm trk}$ multijet control sample, the μ and $\mu_{\rm trk}$ are required to have the same charge. For the ee channel, the electrons must fail isolation and shower shape requirements. The resulting trigger bias is corrected by reweighting distributions in lepton $p_{\rm T}$ and η to match an unbiased control sample. Misidentified ICR electrons in the $ee_{\rm ICR}$ channel are selected from a background region of the $\rm NN_{ICR}$ output.

The dominant background process is the production of a Z boson in association with jets, with the Z boson decaying to dileptons (Z+jets). The light-flavor component (Z+LF) includes jets from only light quarks (uds) or gluons. The heavy-flavor component (Z+HF) includes nonresonant $Z+b\bar{b}$ production, which has the same final state as the signal, and $Z + c\bar{c}$. The remaining backgrounds are from top quark pair ($t\bar{t}$) and diboson production. We simulate $ZH \to \ell^+\ell^- b\bar{b}$ and inclusive diboson production with PYTHIA [11] and Z+jets and $t\bar{t} \to \ell^+\nu b\ell^-\bar{\nu}\bar{b}$ processes with ALPGEN [12], using the CTEQ6L1 [13] leading-order parton distribution functions (PDFs). The events generated with ALPGEN are input to PYTHIA for

parton showering and hadronization, and can contain additional jets. For these events, we use a matching procedure to avoid double counting partons produced by ALPGEN and those subsequently added by the showering in PYTHIA [12]. All samples are processed using a detector simulation program based on GEANT3 [14], and the same offline reconstruction algorithms used to process the data. Events from randomly chosen beam crossings are overlaid on the simulated events to reproduce the effect of multiple $p\overline{p}$ interactions and detector noise.

The cross section and branching ratio for the signal are taken from Refs. [15, 16]. For the $t\bar{t}$ and diboson processes, the cross sections are taken from MCFM [17], calculated at next-to-leading order (NLO). The inclusive Z boson cross section is scaled to next-to-NLO [18], with additional NLO heavy-flavor corrections calculated from MCFM applied to $Z + b\bar{b}$ and $Z + c\bar{c}$.

Corrections are applied to the simulated events to improve the modeling. The simulated $ee_{\rm ICR}$, $\mu\mu$ and $\mu\mu_{\rm trk}$ events are weighted by trigger efficiencies measured in data. For the ee channel, no correction is applied as the combination of lepton and jet triggers is nearly 100% efficient. Lepton identification efficiencies are corrected as a function of $\eta_{\rm det}$ and ϕ of the lepton. Jet energies are modified to reproduce the resolution observed in data. Scale factors are applied to correct for differences in jet reconstruction efficiency between data and simulation. To model the b-tagged samples, simulated events are weighted by their probability to satisfy the ST or DT criteria as measured in data.

The performance of the background model is evaluated in control samples with negligible signal contributions that are obtained by applying only the lepton selection requirements (inclusive) or all selection requirements except b-tagging (pretag). The simulated Z boson events are reweighted such that the $p_{\rm T}$ distribution of the Z boson is consistent with the observed distribution [19]. To improve upon the ALPGEN modeling of Z+jets, motivated by a comparison with the SHERPA generator [20], the pseudorapidities of the two jets with the highest $p_{\rm T}$, and the $\Delta\mathcal{R}$ between them are reweighted to match the distributions measured in the pretag data.

Normalization factors for the simulated and the multijet samples are determined from a fit to the $m_{\ell\ell}$ distributions in the inclusive and pretag data. This improves the accuracy of the background model and reduces the impact of systematic uncertainties that affect pretag event yields (e.g., uncertainties on luminosity). The region $40 < m_{\ell\ell} < 60$ GeV, where the multijet contribution is most prominent, is included in the fit to normalize the multijet control sample to the multijet contribution. The inclusive control sample constrains the lepton trigger and identification efficiencies, while the pretag control sample, which includes jet requirements, constrains a common scale factor $k_{Z+\rm jets}$ that corrects the Z+jets cross section. The total event yields after applying all corrections and normalization factors are shown in Table I.

A multivariate analysis combines the most significant kinematic information into a single discriminant [21]. Each decision tree in a random forest (RF) [22] is trained to separate signal from background using a randomly selected subsample of simulated events. In addition, a random subset of input variables is considered for each decision in each tree. The RF output is a performance-weighted average of the output from each decision tree. To exploit the kinematics of the $ZH \to \ell^+\ell^- b\bar{b}$ process, the energies of the candidate leptons and jets are adjusted within their experimental resolutions with a χ^2 fit that constrains $m_{\ell\ell}$ to the mass and width of the Z boson, and the $p_{\rm T}$ of the $\ell^+\ell^- b\bar{b}$ system to the expected distribution for ZH events before detector resolution effects [7]. The variables selected for the RF are: the transverse momenta of the two b-jet candidates and the dijet invariant mass, before and after the jet energies are adjusted by the kinematic fit; angular differences within and between the dijet and dilepton systems; the angle between the proton beam and the Z boson candidate in the rest frame of the $\ell^+\ell^- b\bar{b}$ system [23]; and composite kinematic variables such as the $p_{\rm T}$ of the dijet system and the scalar sum of the transverse momenta of the leptons and jets. The RF outputs with all lepton channels combined are shown separately for ST and DT events in Figs. 1(a,b).

Systematic uncertainties resulting from the background normalization are assessed for the multijet contribution (20–60% depending on channel) and for effects of lepton efficiency (2-10%), some of which are correlated between all lepton channels (6%). The normalization of the Z+jets sample to the pretag data constrains the Z+jets cross section multiplied by any jet-dependent efficiency to within the statistical uncertainty of the pretag data (1–2%). Additional systematic uncertainties (10–20%) for possible jet-dependent efficiency effects absorbed into $k_{Z+\rm jets}$ are applied to the $t\bar{t}$, diboson and ZH samples. The normalization to the pretag data, which is dominated by Z+LF, does not strongly constrain the cross sections of other processes. A cross section uncertainty of 20% for Z+HF and 6%–10% for other backgrounds is determined from Ref. [17]. For the signal, the uncertainty is 6% [15]. The normalization to the dilepton mass distributions reduces the impact of many of the remaining systematic uncertainties on the background size (except those related to b-tagging), but changes to the shape of the RF output distribution persist and are accounted for. Additional sources of systematic uncertainty include: jet energy scale, jet energy resolution, jet identification efficiency, b-tagging and trigger efficiencies, PDFs, data-determined corrections to the model for Z+jets, and modeling of the underlying event. The uncertainties from the factorization and renormalization scales in the simulation of Z+jets are estimated by scaling these parameters by factors of 0.5 and 2.

No significant excess above the background expectation is observed. Therefore, we set limits on the ZH production cross section with a modified frequentist (CLs) method that uses a negative log likelihood ratio (LLR) of the signal-plus-background (S+B) hypothesis to the

	Data	Total Background	Multijet	Z+LF	Z+HF	Other	ZH
inclusive	865254	853976	131905	701516	19074	1481	9.14
pretag	31336	30634	3449	23234	3459	491	6.82
ST	728	707 ± 130	48.4	161	443	54.1	1.87 ± 0.25
DT	485	435 ± 68	29.5	106	237	61.8	2.34 ± 0.36

TABLE I: Expected and observed event yields for all lepton channels combined after requiring two leptons (inclusive), after also requiring two jets (pretag), and after requiring at least one tight (ST) or two loose (DT) b-tags. The total statistical and systematic uncertainties are indicated for the "Total Background" and "ZH" columns of the ST and DT samples. The "Other" column includes diboson and $t\bar{t}$ event yields. The ZH sample yields are for $M_H = 115$ GeV.

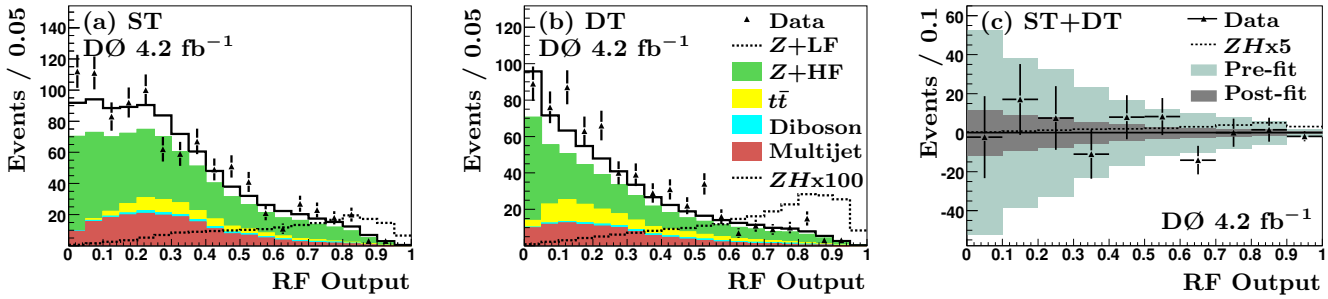

FIG. 1: Data and background RF outputs trained for a Higgs boson with $M_H = 115$ GeV in (a) ST and (b) DT samples. The (c) background-subtracted combination of ST and DT samples, with the systematic uncertainty bands before and after the fit performed by the limit-setting program.

background-only (B) hypothesis [24]. The RF output distributions and corresponding systematic uncertainties of the ST and DT samples from each leptonic channel and from two distinct data taking periods are analyzed separately by the limit setting program to take advantage of the sensitivity in the more discriminating channels. To minimize the impact of the systematic uncertainties, the likelihood of the B and S+B hypotheses are each maximized by independent fits that vary nuisance parameters used to model the systematic effects [25]. The correlations among systematic uncertainties are maintained across channels, as well as backgrounds and signal. The background-subtracted RF distribution, combined for all channels, with systematic uncertainty bands both before and after the fitting procedure, is shown in Fig. 1c.

Figure 2 shows the observed LLR as a function of Higgs boson mass. Also shown are the expected (median) LLRs for the B and S+B hypotheses, together with the one and two standard deviation bands of the background-only expectation. A signal-like excess would result in a negative value of observed LLR. The data are consistent with either hypothesis for the entire mass range $100 < M_H < 150$ GeV. The 95% CL upper limit on the cross section times branching ratio, expressed as a ratio to the SM prediction, for each M_H is presented in Table II. At $M_H = 115$ GeV, the observed (expected) limit on this ratio is 5.9 (7.1). Compared to the previous best expected limit in this channel [4], this represents a 40% improvement.

Supplementary material detailing the pretag control sample, the effect of the kinematic fit, and additional

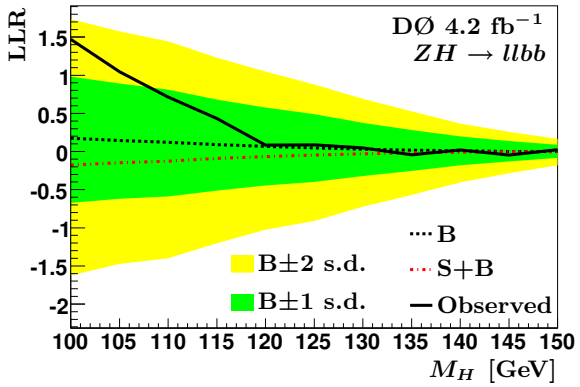

FIG. 2: Observed LLR as a function of Higgs boson mass. Also shown are the expected LLRs for the B and S+B hypotheses, together with the one and two standard deviation (s.d.) bands of the background-only expectation.

cross section limits and LLR distributions from individual lepton channels is available at [26].

We thank the staffs at Fermilab and collaborating institutions, and acknowledge support from the DOE and NSF (USA); CEA and CNRS/IN2P3 (France); FASI, Rosatom and RFBR (Russia); CNPq, FAPERJ, FAPESP and FUNDUNESP (Brazil); DAE and DST (India); Colciencias (Colombia); CONACyT (Mexico); KRF and KOSEF (Korea); CONICET and UBACyT (Argentina); FOM (The Netherlands); STFC and the Royal

M_H (GeV)	100	105	110	115	120	125	130	135	140	145	150
Expected/SM:	5.1	5.6	6.2	7.1	8.4	10.0	12.7	16.8	23.6	34.0	53.6
Observed/SM:	3.0	3.8	4.6	5.9	7.9	9.2	12.1	17.3	22.3	39.4	49.3
Observed (fb):	41	44	44	47	50	45	45	46	41	47	36

TABLE II: The expected and observed 95% CL upper limits on the SM Higgs boson production cross section for $ZH \to \ell^+\ell^- b\bar{b}$, expressed as a ratio to the SM cross section. The corresponding observed limits on the ZH production cross section multiplied by the branching ratio of $H \to b\bar{b}$ are also reported (in fb).

Society (United Kingdom); MSMT and GACR (Czech Republic); CRC Program and NSERC (Canada); BMBF and DFG (Germany); SFI (Ireland); The Swedish Research Council (Sweden); and CAS and CNSF (China).

[a] Visitor from Augustana College, Sioux Falls, SD, USA.
[b] Visitor from the University of Liverpool, Liverpool, UK.
[c] Visitor from SLAC, Menlo Park, CA, USA.
[d] Visitor from ICREA/IFAE, Barcelona, Spain.
[e] Visitor from Centro de Investigacion en Computacion - IPN, Mexico City, Mexico.
[f] Visitor from ECFM, Universidad Autonoma de Sinaloa, Culiacán, Mexico.
[g] Visitor from Universität Bern, Bern, Switzerland.

[1] V.M. Abazov *et al.* (D0 Collaboration), Phys. Rev. Lett. **104**, 071801 (2010).
[2] V.M. Abazov *et al.* (D0 Collaboration), Phys. Rev. Lett. **102**, 251801 (2009)
[3] V.M. Abazov *et al.* (D0 Collaboration), Phys. Lett. B **655**, 209 (2007).
[4] T. Aaltonen *et al.* (CDF Collaboration), Phys. Rev. D **80**, 071101 (2009).
[5] V. M. Abazov *et al.* (D0 Collaboration), Nucl. Instrum. Methods Phys. Res. Sect. A **565**, 463 (2006); M. Abolins. *et al.*, Nucl. Instrum. Methods Phys. Res. Sect. A **584**, 75 (2008); R. Angstadt *et al.*, arXiv:0911.2522 [physics.ins-det], accepted for publication in Nucl. Instrum. Methods Phys. Res. Sect. A.
[6] Coordinates are relative to the proton beam direction, with polar angle θ, azimuth ϕ, and pseudorapidity $\eta = -\ln(\tan(\theta/2))$.
[7] E. A. Strauss, FERMILAB-THESIS-2009-29 (2009).
[8] B. Calpas, FERMILAB-THESIS-2010-23 (2010).
[9] G. C. Blazey *et al.*, arXiv:hep-ex/0005012.
[10] V. M. Abazov *et al.* (D0 Collaboration), Nucl. Instrum. Methods Phys. Res. Sect. A **620**, 490 (2010).
[11] T. Sjöstrand, S. Mrenna, and P. Skands, J. High Energy Phys. **05**, 026 (2006). Version 6.409 was used.
[12] M. L. Mangano *et al.*, J. High Energy Phys. **07**, 001 (2003). Version 2.11 was used.
[13] J. Pumplin *et al.*, J. High Energy Phys. **07**, 012 (2002).
[14] R. Brun, F. Carminati, CERN Program Library Long Writeup W5013 (1993).
[15] J. Baglio and A. Djouadi, CERN-PH-TH-2010-051 arXiv:1003.4266 [hep-ph].
[16] A. Djouadi, J. Kalinowski and M. Spira, Comput. Phys. Commun. **108**, 56 (1998).
[17] J.M. Campbell and R.K. Ellis, Phys. Rev. D **60**, 113006 (1999).
[18] R. Hamberg, W.L. van Neerven and W.B. Kilgore, Nucl. Phys. B **359**, 343 (1991), [*Erratum ibid.* B **644**, 403 (2002)].
[19] V. M. Abazov *et al.* (D0 Collaboration), Phys. Rev. Lett. **100**, 102002 (2008).
[20] T. Gleisberg *et al.*, J. High Energy Phys. **02**, 056 (2004); J. Alwall *et al.*, Eur. Phys. J. C **53**, 473 (2008).
[21] L. Ancu, FERMILAB-THESIS-2010-27 (2010).
[22] A. Hoecker *et al.*, arXiv:physics/0703039 [physics.data-an].
[23] S. Parke and S. Veseli, Phys. Rev. D **60**, 093003 (1999).
[24] T. Junk, Nucl. Instrum. Methods Phys. Res., Sect. A **434**, 435 (1999); A. Read. J. Phys. G **28** 2693 (2002).
[25] W. Fisher, FERMILAB-TM-2386-E (2007).
[26] See supplementary material in the appendix.

Supplementary Material

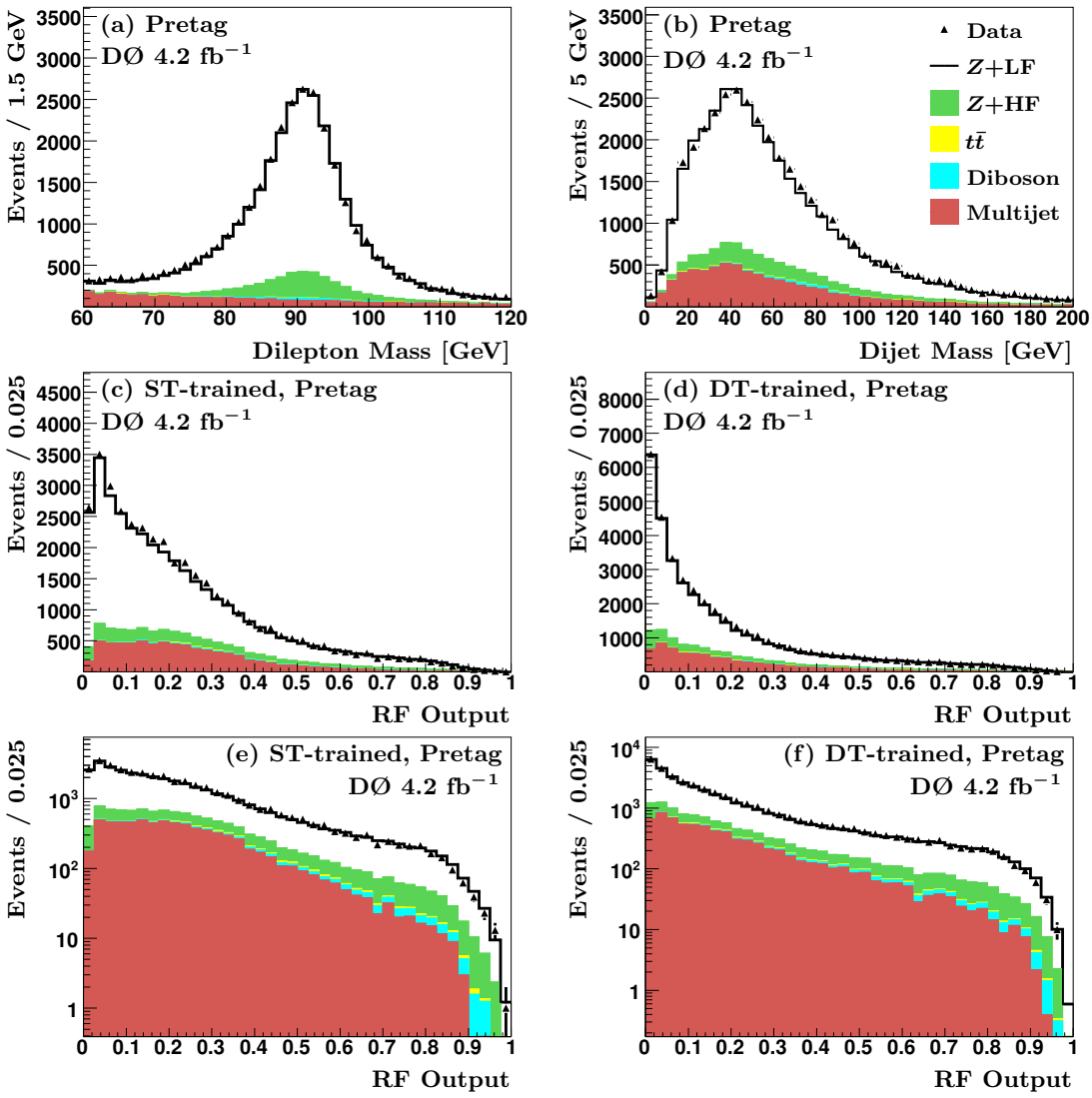

FIG. 3: Pretag distributions for (a) the dilepton invariant mass, (b) the dijet invariant mass after the kinematic fit, (c) the RF discriminant trained for ST events, (d) the RF discriminant trained for DT events, for all lepton channels combined. (e) and (f) reproduce (c) and (d) using a logarithmic scale.

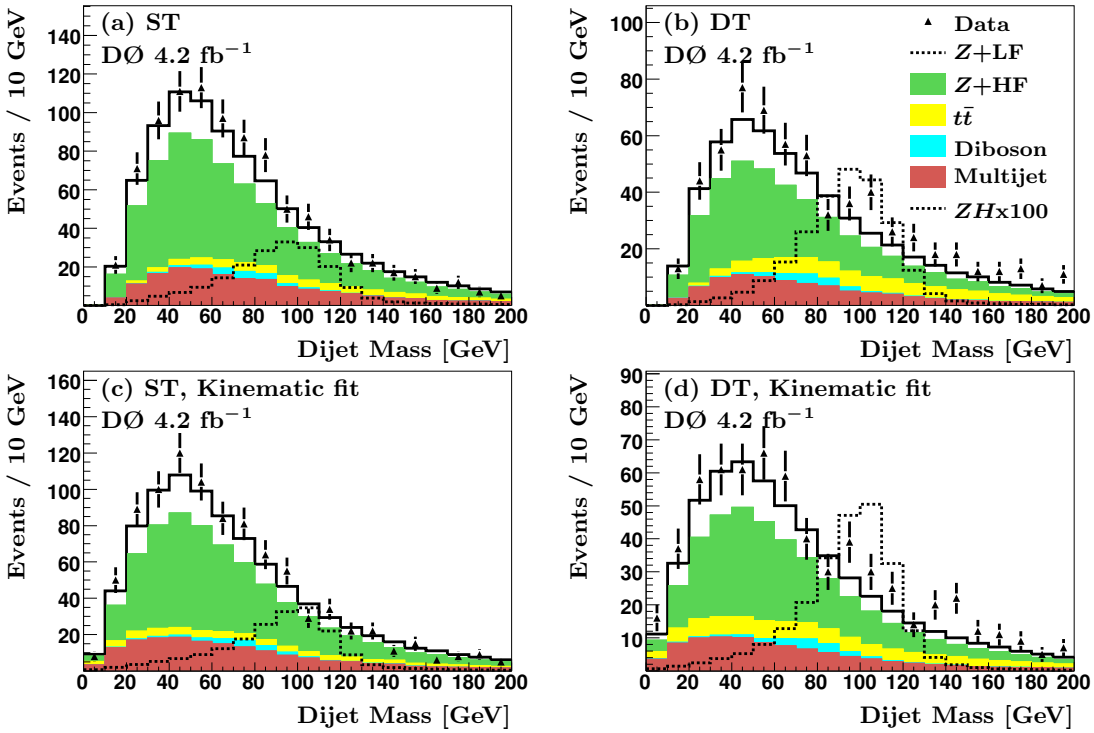

FIG. 4: Dijet invariant mass distributions before the kinematic fit in (a) ST events, and (b) DT events; and calculated from jet energies as adjusted by the kinematic fit in (c) ST events and (d) DT events combined for all lepton channels. The ZH signal shown is for $M_H = 115$ GeV.

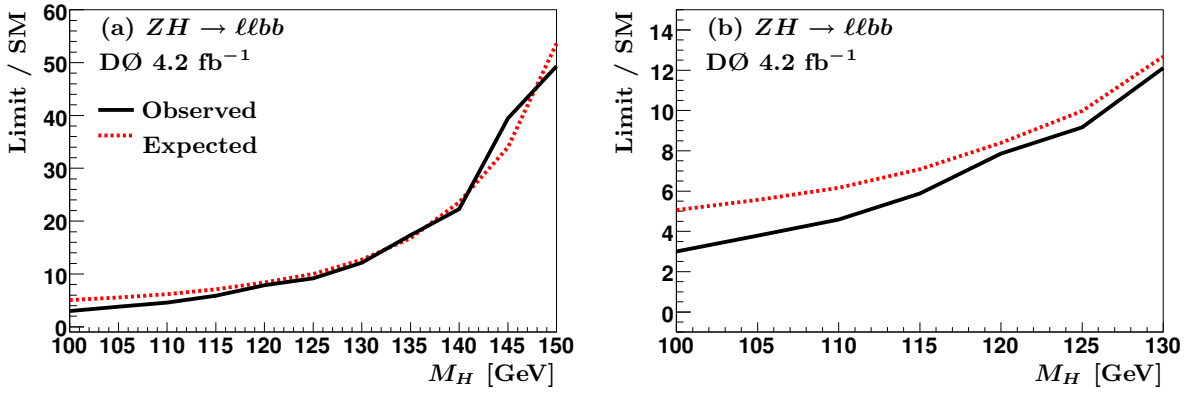

FIG. 5: The expected and observed 95% C.L. cross section limit divided by the SM Higgs boson production cross section as a function of M_H (a) for $M_H \leq 150$ GeV and (b) for $M_H \leq 130$ GeV. Limits are for the combination of the DT and ST samples in all lepton channels.

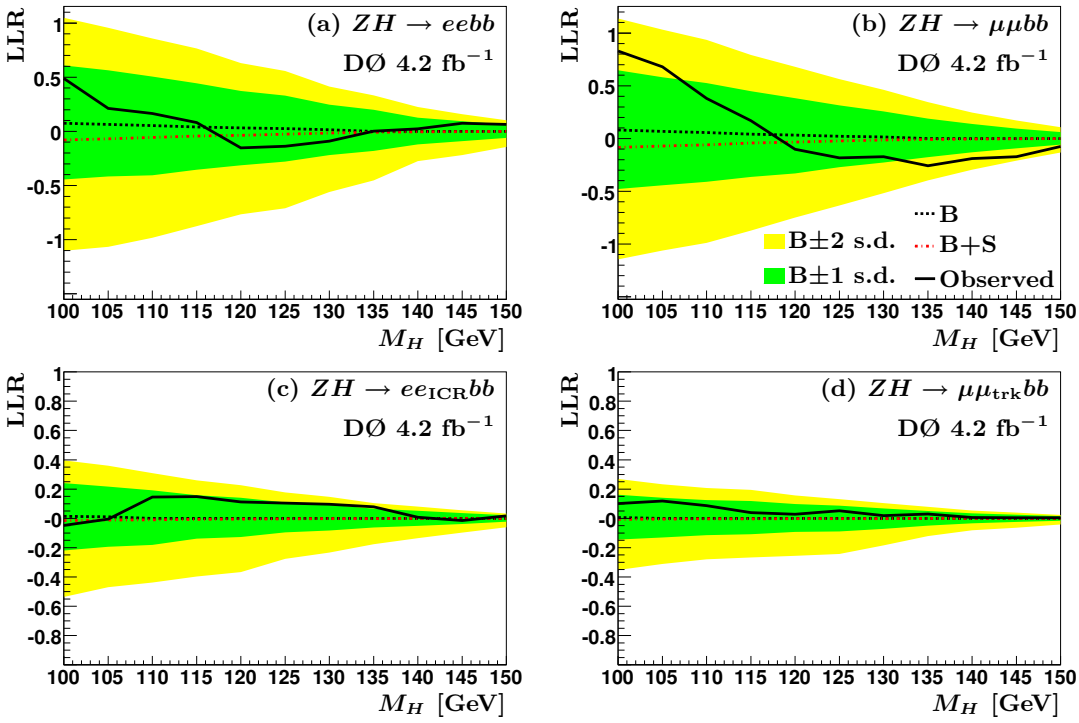

FIG. 6: Observed LLR as a function of M_H for the (a) ee, (b) $\mu\mu$, (c) $ee_{\rm ICR}$, and (d) $\mu\mu_{\rm trk}$ channels. Also shown are the expected LLRs for the B and S+B hypotheses, together with the one and two standard deviation (s.d.) bands about the background-only expectation.

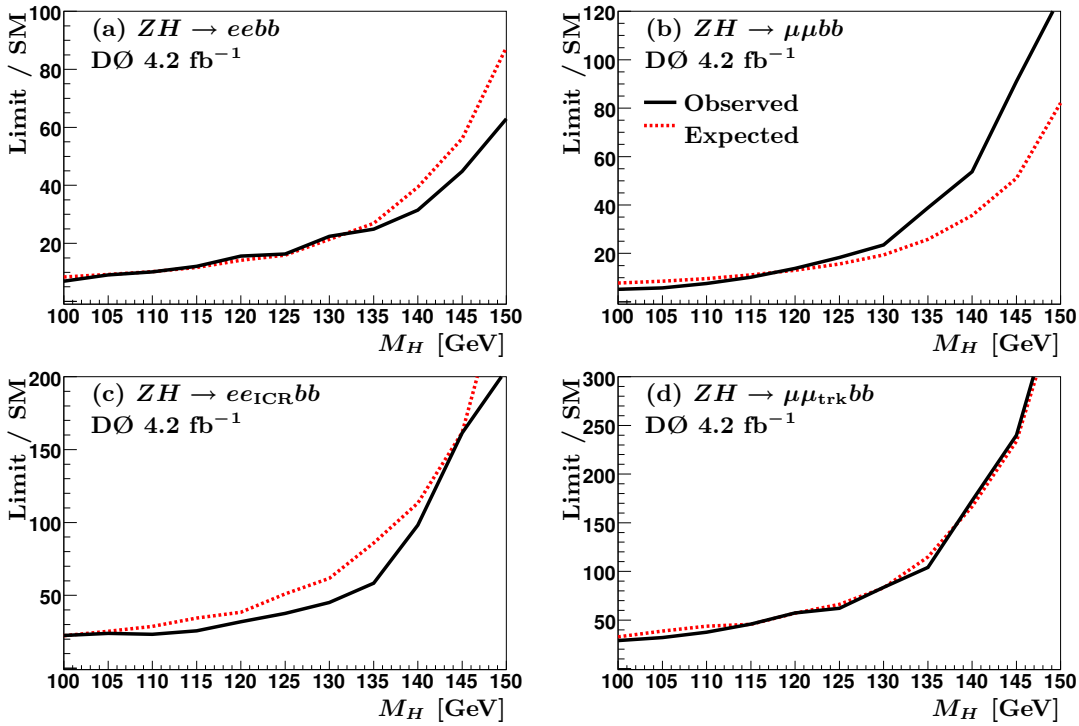

FIG. 7: Expected and observed 95% CL cross section limit divided by the SM cross section as a function of M_H for the (a) ee, (b) $\mu\mu$, (c) $ee_{\rm ICR}$, and (d) $\mu\mu_{\rm trk}$ channels.